Inter- and Intramolecular Interactions in Imidazolium Protic Ionic Liquids

ARTICLE *in* THE JOURNAL OF PHYSICAL CHEMISTRY B · JUNE 2014

Impact Factor: 3.3 · DOI: 10.1021/jp412352k · Source: PubMed

3 AUTHORS, INCLUDING:

Anastasia Maria Moschovi
Institute of Chemical Reaction Engineering
9 PUBLICATIONS **84** CITATIONS
SEE PROFILE

Vassilios Dracopoulos
Foundation for Research and Technology - Hel…
72 PUBLICATIONS **834** CITATIONS
SEE PROFILE

THE JOURNAL OF PHYSICAL CHEMISTRY B

Article

pubs.acs.org/JPCB

Inter- and Intramolecular Interactions in Imidazolium Protic Ionic Liquids

Anastasia Maria Moschovi,[†,‡] Vassileios Dracopoulos,*[,‡] and Vladimiros Nikolakis*[,§]

[†]Department of Chemical Engineering, University of Patras, Karatheodori 1, University Campus, GR-26500 Patras, Greece

[‡]Foundation for Research & Technology Hellas, Institute of Chemical Engineering Sciences, FORTH/ICE-HT, Stadiou Str., Platani, P.O. Box 1414, GR-26504 Patras, Greece

[§]Catalysis Center for Energy Innovation, Department of Chemical and Biomolecular Engineering, University of Delaware, Newark, Delaware 19716, United States

Supporting Information

ABSTRACT: The interactions of alkyl substituted imidazolium bis-(trifluoromethanolsulfonyl)imide protic ionic liquids (PILs) HC_nImNTf_2 (n = 0−12) were studied using vibrational spectroscopy (FT-IR/ATR and FT-Raman) and differential scanning calorimetry (DSC). The effect of alkyl substituent length (n = 0−12) and temperature on the relative magnitude of the different interactions is elucidated. For short carbon alkyl chains (n < 3), the PIL structure is affected from intramolecular interaction caused from the induction effect (+I) due to the chain substituent of the imidazolium ring, while for PILs with n > 3 the van der Waals forces between the chains and $\pi-\pi$ interaction between neighboring imidazolium rings become important. The tendency of reducing the melting point and increasing glass transition values with the lengthening of the alkyl chain was also noticed as a result the increasing contribution of the van der Waals forces to the overall interactions. Finally, we also show that the conformational isomerism of the anion (expressed by ΔH_{eq}) is a good indicator of the relative magnitude of the interactions. When Coulombic interactions are predominant, the *trans* conformer is the most probable, while when other type of interactions (HB, vdW, etc.) become important the *cis* conformer is favored.

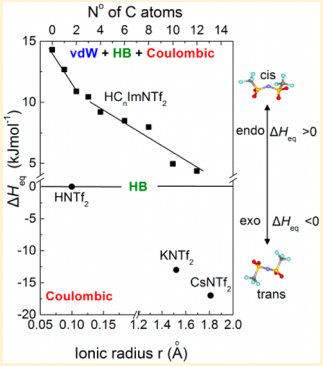

INTRODUCTION

The properties of ionic liquids (ILs) (e.g., low volatility and melting point, wide electrochemical windows, etc.) render them as a promising class of materials for a wide range of applications in catalysis,[1] electrochemistry,[2,3] photovoltaics,[4] or as green solvents.[5] Their structure and physicochemical properties depend on the balance of several types of interactions between the ions such as Coulombic, various dipole, electron pair donor−acceptor, and hydrogen bonds.[6] The contribution of each one to the total interaction energy has recently been estimated using quantum chemical computations. Even though the dispersion forces contribute ∼10%, they have a profound impact on the ability of the anions and the cations to adopt different configurations.[6−8] Furthermore, in order to select the most suitable IL from the almost countless numbers of structures available, it is necessary to link their properties to their structure, which in turn depends on the inter- and intramolecular interactions.[9]

ILs with imidazolium based cations comprise a subcategory that has been extensively used in previous studies (Figure 1). Most of them focused on aprotic ionic liquids (AILs), in which the substitutions in positions 1 and 3 were alkyl groups, while the substitutions in positions 2, 4, and 5 were either hydrogen atoms or alkyl groups. The ions of AILs interact via Coulombic, van der Waals (vdW), and hydrogen bond (HB) forces, thus forming directional bonding between the constituent ions.[10] This is in contrast to their high temperature analogue halide molten salts which mainly form more well-defined coordinated species.[11]

Imidazolium AILs with bis(trifluoromethanolsulfonyl)imide (NTf_2^-) anion are ideal systems for studying interactions, because NTf_2^- has several hydrogen bond acceptor sites. In particular, hydrogen bonds can be formed between the H atoms in sites 2, 4, and 5 of the imidazolium ring and the N or O atoms of NTf_2^-. As a result, substitution of alkyl groups in these sites affects their physical properties (e.g., melting point, viscosity, etc.).[12−15]

In addition, the balance between the electrostatic and van der Waals interactions changes with increasing alkyl chain length on site 1. After a certain length, vdW interactions are responsible for the creation of polar and nonpolar nanophase regions in the liquid phase.[11] Polar regions consist of polar heads of the cation and anions, whereas nonpolar regions consist of alkyl chain aggregates.[13,16]

All previous studies reveal that the properties of ILs and their local molecular environment are in close relation; hence, in this work, we studied the interactions of protic ionic liquids (PILs).[17−19] PILs are a different subset of ILs which are formed

Received: December 17, 2013
Revised: June 27, 2014

   dx.doi.org/10.1021/jp412352k | J. Phys. Chem. B XXXX, XXX, XXX−XXX

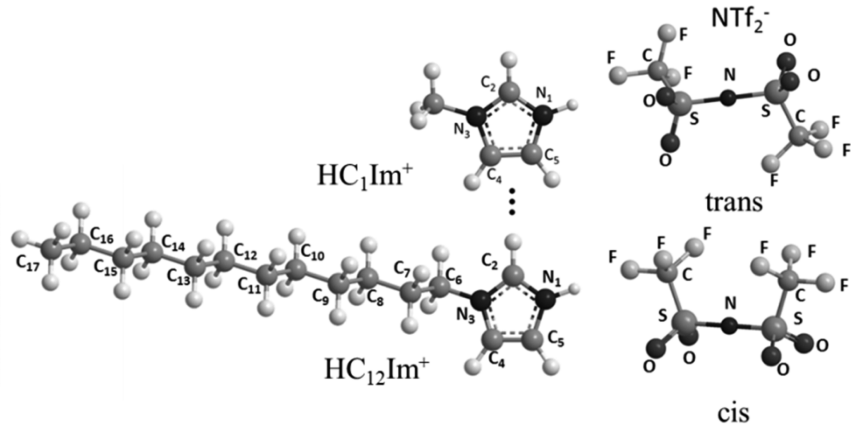

Figure 1. Molecular structure of the cation HC_nIm^+ for n = 0−12 and the conformations of the anion NTf_2^-.

by the reaction between a Brønsted base and a Brønsted acid. The main characteristic of the imidazolium based PILs is the presence of a proton on site 1 of the imidazolium ring (H_1). As a result, PILs can form an extensive network of hydrogen bonds. The systems that we chose for this study are alkyl substituted imidazolium bis(trifluoromethanolsulfonyl)imide ($HC_nIm^+NTf_2^-$ (n: 0−12)) PILs. Schematics of all the cations HC_nIm^+ (n = 0−12) and the isomers of the anion NTf_2^- of all the ILs studied are shown in Figure 1. The anion NTf_2^- can exist in two conformational isomers, *cis* and *trans*.[20,21] In the *cis* conformation, CF_3 groups lay on the same side of the S−N−S bond, whereas, in the *trans* conformation, the groups lay on the opposite side of the bond. The conformation of the anion NTf_2^- shows a significant dependence on the HB strength, since the ions of the PILs studied interact with a well-defined hydrogen bond between the cation and the proton acceptor sites of NTf_2^-.

On the other hand, the aliphatic chain can also exist in different conformers. An alkyl group, attached to the N_3 atom of the ring, rotating around the C_6−N_3 or any C_i−C_{i+1} (i = 6−16) bond, exhibits two isomers, *gauche* (G) and *trans* (T). The two isomers differ in the rotation of the alkyl chain around the C_6−N bond approximately by 106°, as shown in Figure 2.[22]

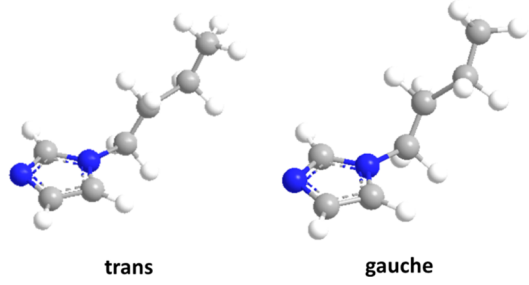

Figure 2. Conformation of the alkyl chain in the cation HC_4Im^+.

The structure of longer alkyl chains is described by the isomerization of C_i−C_{i+1} bonds in the raw, GTTT, TTTT, etc. Since the conformation of the side alkyl chain does not involve any of the H-bonding donors of the imidazole ring, it is not expected to play a significant role on the HB donor capabilities.[7]

Vibrational spectroscopy was used to study the local structure and thus the local interactions between the ions. We focused on the systematic study of the effect of the alkyl chain to the local structure and ion interactions of imidazolium PILs. Raman and FT-IR/ATR spectra from HC_nImNTf_2 (n = 0−12) PILs at room and elevated temperatures were recorded in order to reveal the local structure as well as the effect of local interactions due to alkyl chain on the conformational isomerism of the anion. To elucidate the role of H bonding on the NTf_2^- isomerism, we also carried out similar experiments using alkali metal salts that have only Coulombic interactions. Also, the basic thermodynamic macroscopic parameters like ΔH_m, T_m, and T_g were measured by using differential scanning calorimetry (DSC) and the results will be discussed together with the findings from the vibrational spectroscopic study.

EXPERIMENTAL SECTION

Preparation of the Protic Ionic Liquids HC_nImNTf_2 (n = 0−12) and $ANTf_2$ (A: K, Cs) Molten Salts. Brønsted bases in liquid form 1-alkyl-imidazole C_nIm (n = 2, 3, 6, 8, 10, 12) >98% were purchased from IoLiTec (Ionic Liquids Technologies) GmbH, Brønsted base imidazole Im >99.5% in solid form (flakes) was purchased from Sigma-Aldrich Co., whereas *H*-bis(trifluoromethanolsulfonyl)imide $HNTf_2$ >99% was purchased from Acros Organics.

The synthesis of the protic ionic liquids was carried out under inert conditions in a glovebag (Atmosbag) purchased from Sigma-Aldrich Co. by mixing equimolar quantities of base and acid according to the following stoichiometric reaction

$$HNTf_2 + C_nIm \rightarrow HC_nIm^+ NTf_2^- \quad (1)$$

$KNTf_2$ of 99% purity was provided from Solvionic, while $CsNTf_2$ salt was synthesized in our lab, using carbonate cesium salt Cs_2CO_3 >99.99% purchased from Alfa Aesar according to reaction 2.

$$2HNTf_2 + Cs_2CO_3 \rightarrow 2CsNTf_2 + H_2O + CO_2\uparrow \quad (2)$$

Appropriate amounts of carbonate salt Cs_2CO_3 and $HNTf_2$ were dissolved in anhydrous methanol (Merck) in a glovebag under inert conditions. The solution was then exposed to the atmosphere and was kept under stirring until methanol was evaporated. The crystals were then collected and dried under a vacuum in quartz tubes.

All chemicals, before and after the synthesis procedure, were stored in a desiccator at room temperature, under inert conditions. For Raman spectroscopic studies, all of the chemicals (except $HNTf_2$) studied were dried under a vacuum at 60 °C. Protic ionic liquids were introduced into quartz cells

dx.doi.org/10.1021/jp412352k | J. Phys. Chem. B XXXX, XXX, XXX−XXX

Table 1. Temperatures (°C) of FT-Raman Spectra Recorded for PILs and $ANTf_2$ (A: H, K, Cs)

HC_0ImNTf_2	HC_1ImNTf_2	HC_nImNTf_2 (n = 2−12)	$HNTf_2$	$KNTf_2$	$CsNTf_2$
	60	25	65	220	140
90	90	60	100	245	165
120	120	90	130	270	190
150	150	120	160	295	215
					240

(OD, 6 mm; ID, 4 mm) and sealed under vacuum in a homemade glassy vacuum line. Alkali metal salts $ANTf_2$ (A: K, Cs) and acid $HNTf_2$ were introduced into Pyrex cells (ID, 0.5 mm; OD, 1 mm) and sealed under vacuum as well.

The water content of the PILs was determined after the acquisition of all spectra using Karl Fisher titration. The ionic liquids were dissolved in anhydrous methanol (Merck), and each solution was titrated with an automatic Metrohm 633 titrator (Merck Karl Fischer reagent 5, single component with pyridine 1 mL = 5 mg of H_2O). The water uptake for the PILs tested was estimated between 0.00013 and 0.005% w/w. Details about the water content of each sample are listed in Table S.I.1 of the Supporting Information.

FT-Raman Measurements. Two Raman systems were utilized for the temperature measurements (Table 1) of ILs and molten salts. **System 1:** A FT-Raman system. The FT-Raman spectra were recorded with a BRUKER FRA106/S module on an EQUINOX 55 spectrometer using a NIR excitation line at 1064 nm from an R510 diode pumped Nd:YAG laser (250 mW). The Raman light was collected in the 180° configuration and analyzed by an FT-interferometer equipped with a LN_2 cooled CCD. The spectra were collected as a superposition over 200 scans having a resolution of 4 cm^{-1} and an acquisition time of ∼1.3 s per scan. A homemade optical furnace and temperature controller specially designed for the FT-Raman system was used for the spectroscopic study at elevated temperatures.[23] **System 2:** A UV-Raman system. The spectra of the alkali salts and the $HNTf_2$ at room temperatures and at elevated temperatures were recorded with a high resolution UV-Raman Labram HR-800 spectrograph (JY, ISA Horiba group). In the case of $HNTf_2$ and alkali molten salts, UV-Raman setup was more suitable than a FT-Raman system, due to the presence of the blackbody radiation effect at elevated temperatures. As an excitation source, a 441.6 nm laser line (80 mW) from an air-cooled HeCd laser from KIMMON Electric Co. Ltd. was used. The laser line was focused on the sample with a 50× objective lens (NA = 0.55) through a microscope. The scattered light was then collected in a backscattered geometry and analyzed by a single monochromator equipped with a LN_2 cooled CCD. The spectral resolution was 2.7 cm^{-1}, and the integration time for the spectra was 2 × 150 s. The high temperature Raman spectra were measured using a heating microscope stage (THMS600/720, Linkham Scientific Instruments Ltd.) under the Raman microscope objective. The temperatures were controlled with a TMS93 Linkam Ltd. temperature controller.

Both Raman systems were calibrated before each set of measurements. The FT-Raman system was calibrated with a sulfur standard, while the UV-Raman, with a silicon wafer standard. For the polarization measurements in the liquid state, a CCl_4 sample was used for calibrating the depolarization ratio of the two setups.

Two polarization configurations were used for the Raman spectra of the liquids and melts: vertical−vertical (VV) and vertical−horizontal (VH). The corresponding intensities $I_{VV}(\omega)$ and $I_{VH}(\omega)$ at frequency shift ω were used for the calculation of the isotropic and anisotropic spectra according to the equations

$$I_{ISO}(\omega) = I_{VV}(\omega) - \frac{4}{3}I_{VH}(\omega); \quad I_{ANISO}(\omega) = I_{VH}(\omega)$$

The reduced Raman intensity $R_s(\omega)$, where s stands for VV, ISO, and VH (ANISO), related to the $I_s(\omega)$ according to the relation

$$R_s(\omega) = I_s(\omega)\omega(\omega_0 - \omega)^4[n(\omega) + 1]^{-1}$$

where ω_0 is the excitation frequency and $[n(\omega) + 1]$ is the Boltzmann thermal population factor. The advantages of this spectral representation are expressed elsewhere.[23]

FT-IR/ATR Measurements. FT-IR/ATR spectra of PILs (HC_nImNTf_2) with n between 2 and 12 were collected at room temperature, while, for PILs with n = 0 and 1, spectra were obtained above their corresponding melting points. All spectra were collected using a Bruker Equinox 55 spectrometer, equipped with a single reflection diamond ATR attachment (model: MKII Golden Gate, SPECAC Ltd.). The ATR attachment had KRS-5 lenses, enabling the acquisition of spectra from 400 cm^{-1}. Each sample was placed on the diamond crystal, and the surface was entirely covered with a thin film of HC_nImNTf_2. For the samples with n = 0 and 1, the liquid film was formed at temperatures of 73 and 52 °C, respectively. Spectra were recorded using a 4 cm^{-1} resolution with 200 scans under a N_2 atmosphere. It is very important to note here that a background spectrum at each measuring temperature was collected just before measuring the spectra of each sample.

DSC Measurements. Differential scanning calorimetry thermograms were obtained using a Q100 calorimeter equipped with a LN_2 cooling accessory from TA Instruments SA. The DSC device was calibrated with an indium standard. The cooling rate was 10 °C/min, while the heating was 5 °C/min and covered the range from −120 to 120 °C. The melting points were calculated on the onset of the endothermic peaks while glass transition temperatures on the midpoint of the glass transition step, as shown in Figure S.I.1 (Supporting Information).

RESULTS AND DISCUSSION

Thermal Properties. The melting points and glass transition temperatures as a function of alkyl chain are presented in Figure 3 (the thermograms of all the PILs studied are shown in Figure S.I.2 as Supporting Information). Melting points were observed for the two ends of alkyl chain length, below four and above eight C atoms in the chain. Glass transition temperatures were measured for all of the PILs except for the two first members of the sequence. The melting points of PILs studied here are also compared with reported values of the corresponding APILs (Table 2).[24] It is clear that

dx.doi.org/10.1021/jp412352k | J. Phys. Chem. B XXXX, XXX, XXX−XXX

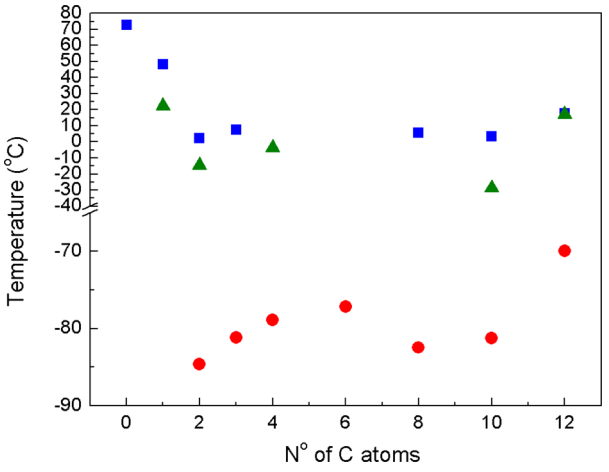

Figure 3. Experimental melting T_m of (■) PILs and (▲) AILs[25] and (●) glass transition T_g temperatures of PILs as a function of the number of C atoms in the alkyl chain.

Table 2. Melting T_m and Glass Transition Points T_g for Protic HC_nImNTf_2 and Aprotic $C_1C_nImNTf_2$ (n = 0−12) ILs[24]

n	T_m for HC_nImNTf_2 (°C)	T_g for HC_nImNTf_2 (°C)	T_m for $C_1C_nImNTf_2$ (°C)
0	72.76		
1	48.15		22.15
2	2.35	−84.65	−14.85
3	7.49	−81.15	
4		−78.87	−3.85
6		−77.14	
8	5.78	−82.47	
10	3.45	−81.21	−28.85
12	17.74	−69.93	16.85

the melting points of PILs are higher compared to those of the APILs, probably due to the additional hydrogen bond between the nitrogen atom of the cation and NTf_2^-,[25] which increases the stiffness of PIL structural units compared to the APILs and could explain the observed behavior.

The glass transition temperature increases as a function of alkyl chain length, indicating that there are segments in the structure that became less mobile. One possible explanation for this effect is the strengthening of the interactions between the side alkyl chains. This implies that the local structure is probably similar to the corresponding APILs where the long alkyl chains form nonpolar domains due to vdW interactions, resulting in less mobile areas and thus the increase of the glass transition temperatures. A local minimum in T_g, observed for n = 8 and 10, is probably caused by the formation of metastable phases, due to conformational or orientation disordering of the alkyl chain.[26] Moreover, the addition of $-CH_2$ groups results in the free volume increase which probably is the reason for the glass transition temperature depression.

The melting point shows a depression up to n = 2, while upon further increase of n its value slightly increases. The fast depression is probably correlated with the number and magnitude of the hydrogen bonds, together with a reduction of the Coulombic interactions between the ions due to the increase of the cation size.[27] This cannot explain the high end of the alkyl chain length studied. If we adopt the explanation proposed in the previous paragraph, then the slight increase of the melting point can be attributed to the increased stiffness of the side alkyl chain. The above discussion indicates that certain structural changes occurred in these PILs with increasing alkyl chain length, which strongly affect their thermal properties. Previous WAXS studies indicated the structural organization of the polar and nonpolar regions to nanostructures, indicating that the separation of the high charged heads from the low charged aliphatic chains results in the formation of low and high density regions.[28,29] This density fluctuation can be reflected in the thermal properties of the ILs.[30] However, unlike vibrational spectroscopy, the thermodynamic measurements give only indications, which can be considered as speculative, about the interactions and local structure. To address this issue, we used vibrational spectroscopy.

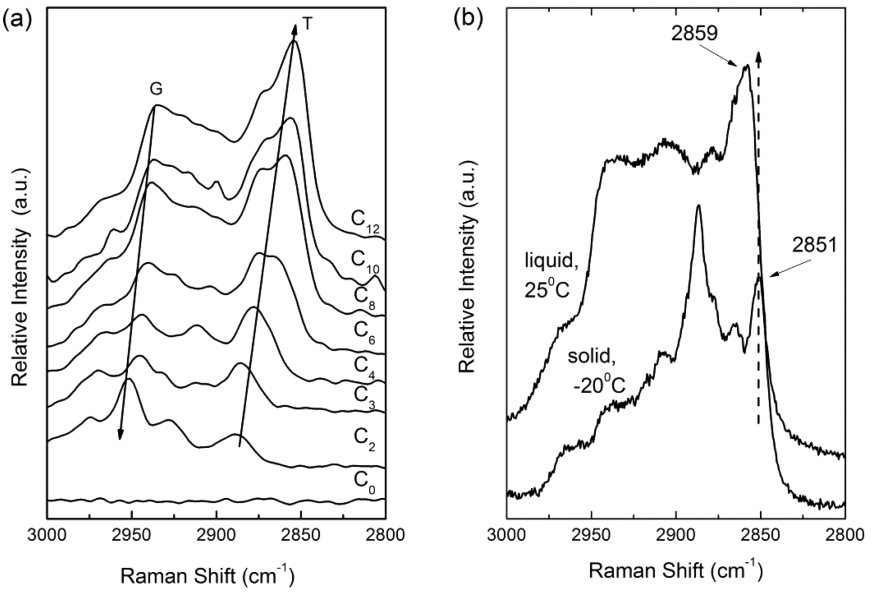

Figure 4. (a) Isotropic Raman spectra for HC_nImNTf_2 (n = 0−12) in the region 3000−2800 cm^{-1}. (b) Raman spectra of the 3000−2800 cm^{-1} spectral region of the $HC_{12}ImNTf_2$ salt in the solid and liquid phases.

dx.doi.org/10.1021/jp412352k | J. Phys. Chem. B XXXX, XXX, XXX−XXX

Effect of Alkyl Chain Length on the Structure of the Cation. The Raman spectra of the alkyl group CH_2 stretching region of all PILs studied are shown in Figure 4a. The intensity of the band assigned to the CH_2 symmetric stretching mode (T band) increases compared to that of asymmetric stretching (G band). These two bands are correlated to the *trans* (T band) and *gauche* (G band) conformations of the alkyl chain. The deconvoluted spectra of this region are shown in Figure S.I.3 (Supporting Information).

Furthermore, the frequencies of both bands continuously shift to lower wavenumbers, reaching the frequencies observed in molten polymethylene[31] and liquid *n*-alkanes,[32] indicating that the alkyl side chain of the imidazole ring probably has a local structure similar to that observed in these melts. This is further supported by the spectra in the solid and liquid $HC_{12}ImNTf_2$ in Figure 4b.

The spectra of the solid $HC_{12}ImNTf_2$ are similar to those observed in solid alkanes and polymethylene in which the alkyl chains are packed in an all *trans* geometry.[31] Due to the similarities of both systems, we assigned the observed bands to the existence of the alkyl chain in the crystal to an all *trans* chain. Upon melting, the symmetric stretching vibration shifts to higher energies of about 8 cm^{-1}. A similar observation in polymethylene was attributed to the appearance of *gauche* defects on the *trans* structure of the alkyl chain. The red shift of the CH_2 symmetric and antisymmetric stretching modes as the alkyl chain size increases is probably due to the reduction of the reorientation ability and flexibility of the side chain. This is consistent with what has been observed in aprotic ILs where the chains are oriented due to vdW interactions introducing nonpolar regions into a polar network.[13,16] Thus, we propose a similar structure model for the protic imidazolium ILs.

Apart from this general observation, a closer view to the local *gauche*/*trans* chain conformations can be given by the external deformation β of the CH_3 at the end of the chain. This mode is localized in the 900−820 cm^{-1} spectral region.[33] This spectral region for the crystalline and liquid phases for $HC_{12}ImNTf_2$ is shown in Figure 5. If the alkyl chain of the solid $HC_{12}ImNTf_2$ is packed in the all *trans* geometry (as hypothesized above), then only the ∼900 cm^{-1} band which corresponds to the TT conformers of the end carbon atoms of the chain should be observed. This is indeed the case in Figure 5.

It is well established that the β deformation vibrational mode of the methyl group at the end of the alkyl chain is strongly affected by the *gauche* defects caused by the carbon atoms of the methylene group close to them. From the pioneer study of the melting of nonadecane hydrocarbons, we expected that, if we have a *gauche* structure between the carbon atoms of the second and third positions (C_{16}−C_{17} TG end chain conformation) of the chain, then a band at ∼870 cm^{-1} should be observed.[34]

If the *gauche* defects lay between the third (C_{16}) and fourth (C_{15}) carbon atoms, then the band is expected to be observed at ∼847 cm^{-1} (GT conformer). In the spectra of the liquid $HC_{12}ImNTf_2$, we observe all the possible configurations of the TT, TG, and GT structures for the end of the chain of the 12 carbon atoms. This shows that the structure of the side chain is quite distorted compared to that of the crystal. The presence of many *gauche* conformers makes the orientational motion of the chains more complicated and of course more difficult. This spectral region for all the PILs measured is presented in Figure 6.

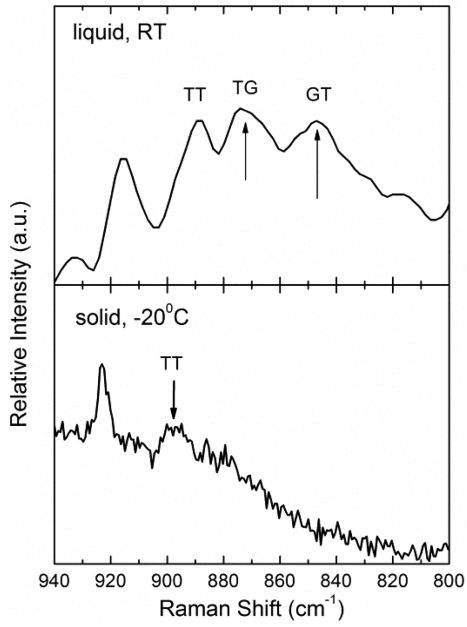

Figure 5. Raman spectra of the 940−800 cm^{-1} spectral region of the solid and liquid phases of $HC_{12}ImNTf_2$.

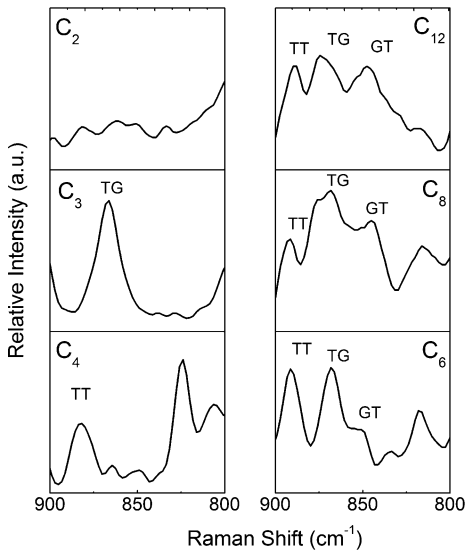

Figure 6. Spectra of the HC_nImNTf_2 in the 900−800 cm^{-1} spectral region where the end chain *gauche* and *trans* defects are.

It is clear that the picture of the *gauche* conformers is more complicated for the longer chains compared to the short ones. It seems that when *n* is higher than 6 all possible conformers exist (in different populations), while when *n* is less than 6 the spectra reveal a more defined local structure. Thus, for the butyl system, the chain ends with a TT conformation, while, for the propyl system, a TG structure is dominant.

Effect of Alkyl Chain Length on Hydrogen Bonding. The observed red shifts of the N−H stretching mode (3270−3250 cm^{-1})[23] and the C−H stretching mode (3170−3150 cm^{-1}) IR frequencies as a function of the alkyl chain length are shown in Figure 7 (the deconvoluted FT-IR spectra of these regions are provided as Supporting Information, Figure S.I.4). The spectra have been smoothed by a FFT filter and 5 points of window using Origin 7.5 software. Considering that the water content of the samples determined after these measurements

dx.doi.org/10.1021/jp412352k | J. Phys. Chem. B XXXX, XXX, XXX−XXX

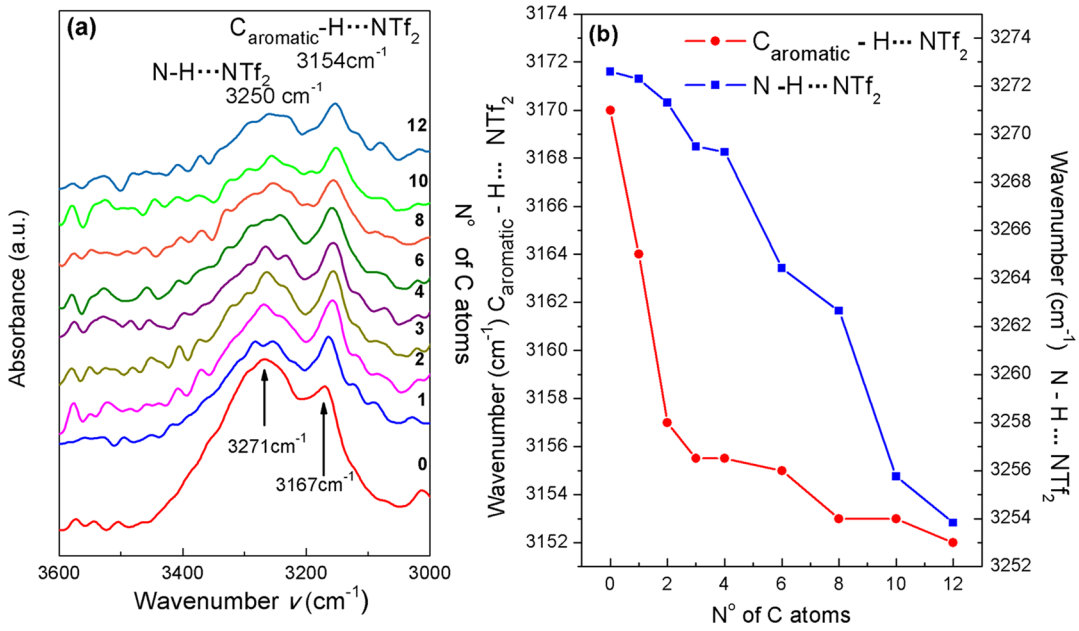

Figure 7. (a) FT-IR/ATR spectra of the HC_nImNTf_2 PILs in the liquid phase at 90 °C (n = 0), 60 °C (n = 1), and 25 °C ($n \geq 2$). (b) Observed FT-IR/ATR frequencies of the (■) N−H modes and (●) $C_{aromatic}$−H as a function of the number of alkyl chain C atoms.

was less than 0.002 wt % (see Table S.I.1 in the Supporting Information), we do not expect to have interference of H_2O vibrational modes in the high frequency spectral region of the N−H···NTf_2^- bonds.

The spectral charachteristics in this area are quite different than those of the corresponding APILs. In addition to the presence of the N−H···NTf_2^- mode, the shape and band characteristics of C_i−H···O (i: 2, 4, or 5) modes are also different. Furthermore, there has been a controversy regarding the assignment of the νC_i−H···O stretching modes. Normally, the FT-IR bands at 3170 ± 15 and 3120 ± 15 cm^{-1} observed in imidazolium APILs are assigned to the $C_{4,5}$−H and C_2−H stretching modes.[35,36] In 2009, Lassegues and co-workers revisited these assignments by taking into account the possibility of a Fermi resonance caused by the overtones/combinations of the ring vibrations at 1500−1600 cm^{-1} with the stretching fundamentals at 3100−3200 cm^{-1}.[35] Their main conclusion was that the high frequency mode has also a C_2−H contribution (in addition to the $C_{4,5}$−H) while the low frequency mode is mainly due to the Fermi resonance. Indeed, the overtone of the ring stretching mode at 1587 cm^{-1} (see paragraphs that follow) overlaps with the stretching vibration of the $C_{aromatic}$−H··· NTf_2^- mode and could result in a Fermi resonance interaction of these two modes. This interpretation sparked a debate between the spectroscopists.[37,38] In a recent publication, Ludwig et al.[39] used nonlinear Raman spectroscopy (CARS: coherent anti-Stokes Raman spectroscopy) to show that the high frequency area is attributed to the $C_{4,5}$−H in-phase and out-of-phase modes while the lower one had contributions from the C_2−H mode and the corresponding Fermi resonance of this mode with the ring modes at 1575 cm^{-1}. These assignments were further supported by recent IR spectra of vapor phase jet-cooled $EMImNTf_2$.[40,41] This study also showed that an assignment of the low frequency band only to a Fermi resonance cannot explain the spectral behavior of the C_2−H band as a function of jet temperature and contribute probably to a further broadening of the observed band. Katsyuba et al. assigned the high frequency mode in the FT-IR spectrum of $C_2OHImPF_6$ to the C_2−H while the lower one to the $C_{4,5}$−H, showing again the difficulties in the assignment of these bands.[42] To address the assignment uncertainties, they adopted the $C_{aromatic}$−H notation for describing these modes. They also suggested that if weak hydrogen bonds are formed then a blue shift can be expected due to secondary effects caused, e.g., by a certain arrangement between the anion and cations (the anion on the top or bottom of the imidazolium ring).

All of the above discussion shows clearly that precise assignment of this spectral area is difficult and extreme care must be taken to avoid misnterpretations. The shape of the 3170−3150 cm^{-1} band shows that probably all of the C_i−H (i: 2, 4, 5) stretching modes of the ring are included in this envelope (this area can be fitted quite well by two Gaussians: one for the N−H···O and one for the $C_{aromatic}$−H···O band). One possible interpretation is that the arrangement between the anion and the cation is in that way resulting in a further blue shift of the C_2−H mode and overlapped by the $C_{4,5}$−H modes.[42] Another approach for these band shape characteristics could be the possible vibrational energy transfer through hydrogen bonds between the C_2−H and $C_{4,5}$−H modes resulting in the enhancement of the lifetime of the receiving mode and reduction of the lifetime of the donating mode.[8,43] In order to avoid any misinterpretation, we will follow the $C_{aromatic}$−H···NTf_2^- notation for this band.[42] If the contibution of the Fermi resonance is important, then the weak absorbance of the $2\nu_S^R$ will be significantly enhanced and probably explain the observed asymmetry on the low frequency part of the $C_{aromatic}$−H···NTf_2^- stretching mode. Theoretical calculations in combination with nonlinear vibrational spectroscopy studies are two possible methods that can be used to shed further light in our interpretation.

In any case, the frequency of the N−H or $C_{aromatic}$−H stretching bands depends on the HB strength between the H atom of the imidazolium ring and NTf_2^- and it can be correlated to the existence of directional interactions between the anions and the cations in the liquid phase. In Figure 7b, we

dx.doi.org/10.1021/jp412352k | J. Phys. Chem. B XXXX, XXX, XXX−XXX

present the shift of the N−H and $C_{aromatic}$−H as a function of the number of C atoms in the alkyl chain. Both modes show a red shift with increasing alkyl chain length even though they do not follow the same trend. More pronounced shifts of the $C_{aromatic}$−H mode are observed when the alkyl chain length *n* is increased from 0 to 3, while the N−H shifts seem to have an almost linear dependence on *n*. One hypothesis is that the shift of the $C_{aromatic}$−H mode can be attributed to the inductive effect of the side alkyl chain to the imidazole ring which in turn affects the hydrogen bond strength of the ring hydrogen atoms with NTf_2^-. The induction effect is also expected to be more pronounced on the $C_{aromatic}$−H bonds, since they are closer to N_3 than the N_1−H bond. Furthermore, its magnitude should depend on the alkyl chain length only for small values of *n*, whereas when $n > 3$ the effect of *n* should be negligible. This seems to be in qualitative agreement with the observed $C_{aromatic}$−H bond shifts shown in Figure 7b, indicating that this vibration is primarily affected by the side chain substituent inductive effect on the ring. However, since the alkyl chains are electron donating groups, the overall positive charge of the imidazole ring should decrease with increasing *n*. Moreover, the group of Kirchner showed that, with increasing alkyl chain length, the distance between the anion and the cation increases as well.[44] As a result, we should expect to see hydrogen bond weakening. Usually, weakening of an X−H···Y hydrogen bond is associated with a blue shift of the X−H vibration instead of the observed red shift with increasing *n*. However, there are numerous examples in the literature demonstrating that it is possible, under certain circumstances, to observe a blue shift of the X−H vibration when an X−H···Y hydrogen bond forms (such hydrogen bonds are often called improper hydrogen bonds).[8,45,46] Thus, if the observed red shift with increasing *n* is attributed to the hydrogen bond weakening due to the inductive effect, then the $C_{aromatic}$−H bonds of the imidazolium ring probably form improper hydrogen bonds (blue-shifted) with NTf_2^-. However, as discussed earlier, this area probably has contributions due to Fermi resonance of the ring stretching vibrations and the $C_{aromatic}$−H stretching. As a result, the effect of the $C_{aromatic}$−H shifts on the existence and contribution of Fermi resonance bands has also to be considered, and is an area that insights from molecular simulations will be extremely valuable.

The FT-IR C−N ring stretching vibrational mode region of the protonated imidazolium ring for the PILs HC_nIMNTf_2, $n = 0-12$, is shown in Figure 8. The bands at ∼1553 and ∼1587 cm^{-1} correspond to R_2 and R_1 stretching vibrational modes of the protonated cation HIm^+, respectively. The splitting of these bands is higher compared to the corresponding APILs, indicating that the directional HB, between the ions, distorts more the local symmetry of the ring. An abrupt shift to lower energies (∼6 cm^{-1}) is observed when the alkyl chain changes from methyl to ethyl, whereas there is no further shift as the alkyl chain length increases from 2 to 12 (ethyl to dodecyl). The observed frequency jump indicates an increase of the C−N bond distances, which results in the imidazole ring extension. This ring extension does not further change as the alkyl chain increases.

An important question that still has to be answered is why the dependence of the N−H shift on alkyl chain length is different than that of the $C_{aromatic}$−H shift. This observation can be explained if the N−H mode is affected primarily from intercationic interactions like the $\pi-\pi$ interactions between neighboring imidazolium rings. Mignon et al. studied the effect

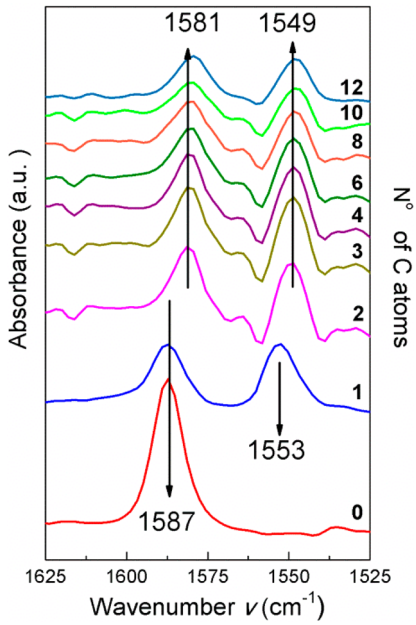

Figure 8. FT-IR/ATR spectra for HC_nImNTf_2 ($n = 0-12$) in the region 1625−1525 cm^{-1}.

of $\pi-\pi$ interactions between monosubstituted benzene rings and imidazole rings.[47] They found that the hydrogen bonding ability of the imidazole ring increases when it is in parallel stacking with benzene groups substituted with electron donating groups (e.g., alkyl chains), while the opposite is observed in the case of T-shaped stacking.

In a similar manner, the observed redshift of the N−H bond which is formed between the proton of the imidazolium ring and NTf_2^- with increasing alkyl chain length reflects the hydrogen bond's strength changes, which can be attributed to a larger fraction of imidazolium rings in parallel stacking.

The latter is also supported by the spectral changes of the C−N stretching modes (Figure 8) which show that there is a ring extension (destabilization) for chains with $n > 2$. Thus, the relative contribution of the intercationic $\pi-\pi$ interactions becomes more important than the intramolecular (+*I* effect) ones.[6,17]

The Anion Conformation Isomerism as a Monitor of Local Interactions. The effect of the intra- and intermolecular forces in the relative populations of the NTf_2^- *trans* and *cis* conformations was also studied. The frequency of the N−H and $C_{aromatic}$−H stretching as a function of the ratio of the populations of the two NTf_2^- conformers (I_{trans}/I_{cis}) is shown in Figure 9. This ratio was calculated from FT-IR normalized spectra of the region of $\nu_{asym}SO_2$ modes (Figure S.I.5, Supporting Information). The normalized FT-IR spectra of symmetric and asymmetric vibrational modes show that the increase of the $-CH_2-$ groups in the alkyl chain favors the *trans* conformation of the anion.

The $C_{aromatic}$−H frequency decreases linearly with I_{trans}/I_{cis}. This, in turn, shows that the population of these two conformers is affected primarily by the intramolecular interactions and to a lesser extent by the interionic $\pi-\pi$ interactions between the rings.

Therefore, it seems that the equilibrium of the NTf_2^- conformers depends on the PIL local interactions. We also investigated the effect of temperature on this equilibrium from the corresponding Raman spectra collected at different

dx.doi.org/10.1021/jp412352k | J. Phys. Chem. B XXXX, XXX, XXX−XXX

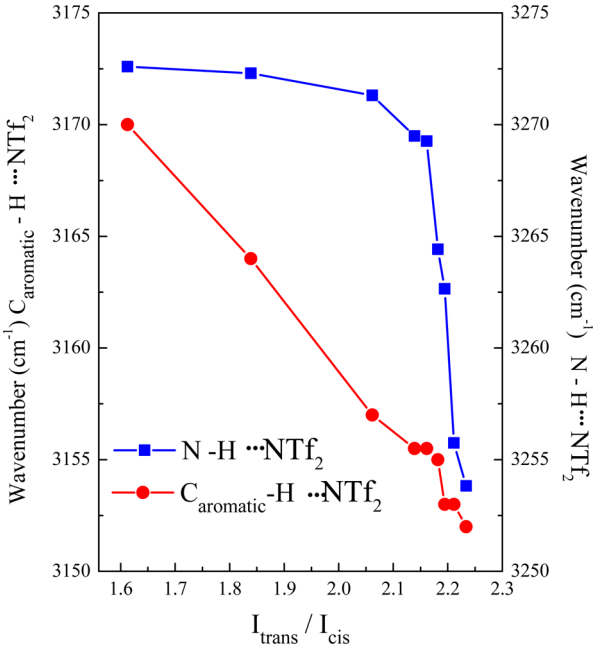

Figure 9. FT-IR/ATR frequencies of the (■) N−H modes and (●) $C_{aromatic}$−H as a function of the ratio of the relative intensities I_{trans}/I_{cis} of the $\nu_{asym}SO_2$ from the normalized FT-IR/ATR spectra of the HC_nImNTf_2 (n = 0−12).

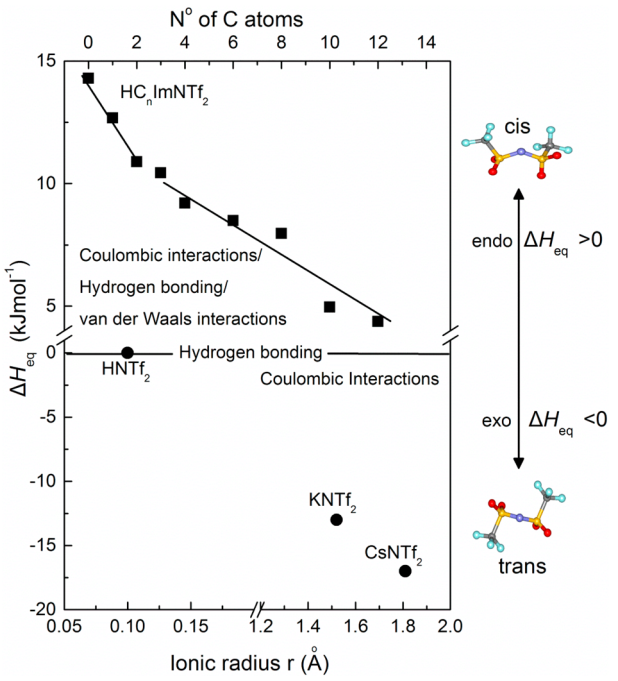

Figure 10. Energy diagram of the ΔH_{eq} values of the protic ionic liquids HC_nImNTf_2 (n = 0−12), alkali metal salts $ANTf_2$ (A: Cs and K), and the strong acid $HNTf_2$ calculated from the analysis of experimental data at different temperatures. The lines are guides for the eye.

temperatures. In the case of HC_nImNTf_2, the *cis* conformer becomes more stable at elevated temperatures. On the other hand, in the case of molten alkali-NTf_2^- salts, we found that the *trans* conformer is favored at elevated temperatures. Finally, in the case of the strong acid $HNTf_2$, no spectral changes were observed, indicating that no changes in conformational equilibrium with temperature can be observed with vibrational spectroscopy. Thus, how does the equilibrium of NTf_2^- conformers "reflect" the local interactions in ILs?

To answer this question, we calculated the ΔH_{eq} of the anion conformational isomerism from the νSO_2 symmetric stretching vibrational mode area (1120−1150 cm^{-1}) of the reduced isotropic Raman spectra. The deconvoluted spectral regions for different temperatures which were used for the ΔH_{eq} calculation for PILs, $ANTf_2$ molten salts, and Brønsted acid $HNTf_2$ are shown in Figure S.I.6−8 (Supporting Information). The methodology of the calculations has been analyzed thoroughly elsewhere.[23] The Arrhenius plots of the van't Hoff equation for the measured PILs are provided as Supporting Information in Figure S.I.9. The ΔH_{eq} values in the case of PILs as a function of C atoms in the alkyl chain and as a function of alkali metal ionic radius are shown in Figure 10 and listed in Table 3.

The most evident observation is the opposite sign of ΔH_{eq} depending on the cation (alkali vs imidazolium). In the case of alkali-NTf_2 molten salts, the *trans* conformation of the anion is favored at elevated temperatures; thus, ΔH_{eq} is negative.

On the contrary, in the case of imidazolium based NTf_2 ILs, the *cis* conformation population increases with temperature, resulting in positive ΔH_{eq} values. However, in both cases, ΔH_{eq} decreases, either with ionic radius or with the alkyl group number of carbon atoms following the same trend as the T_m of the PILs. The decrease with the alkyl chain length is probably due to the reduction of the electrostatic force contribution to the overall interaction between the ions, since the contributions

Table 3. Experimentally Determined ΔH_{eq} Values for the Protic Ionic Liquids HC_nImNTf_2 (n = 0−12) and the Alkaline Molten Salts $KNTf_2$ and $CsNTf_2$

	$\Delta H_{trans\leftrightarrow cis}$ (kJ mol^{-1})
Ionic Liquids	
HC_0ImNTf_2	14.29 ± 1.29
HC_1ImNTf_2	12.59 ± 1.99
HC_2ImNTf_2	10.73 ± 0.94
HC_3ImNTf_2	10.44 ± 1.52
HC_4ImNTf_2	9.72 ± 0.46
HC_6ImNTf_2	8.49 ± 1.08
HC_8ImNTf_2	7.13 ± 0.42
$HC_{10}ImNTf_2$	4.9 ± 0.67
$HC_{12}ImNTf_2$	4.31 ± 0.2
Alkali Molten Salts $ANTf_2$	
$KNTf_2$	−13.86 ± 2.6
$CsNTf_2$	−20.73 ± 2.4

of the other forces (HBs, vdW, dispersion due to $\pi-\pi$ interactions) to the total energy of the pair of ions become more pronounced. Furthermore, in the case of PILs, there is a change of the slope at n = 3. On the high carbon atom chain, the ΔH_{eq} shifts to even lower values, showing a gap and becoming closer to the value predicted by theory for the free rotamer. This probably happens due to the increased distance between the polar heads that leaves space for the anion to rotate more freely.[48] The same trend of the ΔH_{eq} decrease was also observed from calculations from the spectral region of ρSO_2 vibrational modes which is presented in Figure S.I.10 (Supporting Information). For the PILs HC_nImNTf_2, n = 4, 8, 10, it was not possible to calculate the ΔH_{eq} from this low frequency spectral region, due to vibrational modes overlapping.

dx.doi.org/10.1021/jp412352k | J. Phys. Chem. B XXXX, XXX, XXX−XXX

Similar results were shown by Rocha et al.[18] who calculated the enthalpy and entropy change for vaporization (ΔH_{vap} and ΔS_{vap}) of the aprotic ionic liquids $C_1C_nImNTf_2$ as a function of the alkyl chain length (n = 2−12).[18] The changes of the ΔH_{vap} and ΔS_{vap} with alkyl chain length were attributed to the decrease of the electrostatic interactions and the increase of the van der Waals ones with n. They found that for small alkyl chains ($2 < n < 6$) the slope of the calculated values with n is higher than the same slope when n is between 6 and 12. Furthermore, the change of slope at $n = 6$ was attributed to the formation of distinctive polar and nonpolar regions at $n > 6$ instead of isolated islands of nonpolar chains in the continuous polar phase when $n < 6$. On the other hand, according to a more recent study of the aprotic ionic liquids $C_1C_nImNTf_2$ (n = 1−18), the calculated values of the ΔH_{vap} and ΔS_{vap} had a linear dependence on n for $2 < n < 18$, while for $n = 1$ and $n = 2$ both quantities were relatively constant.[19] Furthermore, they showed that the contribution of the electrostatic interactions in the thermodynamic properties reduces more sharply when n is changed from 1 to 2 rather than in the region $2 < n < 18$. Thus, the change in the slope in our experimental ΔH_{eq} values might reflect the change of the most pronounced interaction from intramolecular to interionic. Moreover, the melting points of the PILs, for $n < 3$, show a similar decrease to the values of the ΔH_{eq}, indicating that the $+I$ effect contributes to the depression of the melting points, whereas, for $n > 3$, the dominance of the intermolecular interactions shows no significant effect on the macroscopic properties of the PILs.

CONCLUSIONS

In summary, we showed how the structure and thermal properties of imidazolium PILs are affected by the alkyl side chain length and temperature. We also showed that in all systems studied directional interactions (i.e., hydrogen bonds) are formed. For short carbon alkyl chains ($n < 3$), the molecular structure is affected from intramolecular interaction probably caused from the $+I$ effect of the chain substituent of the imidazolium ring, while for PILs with $n > 3$ the $\pi-\pi$ interaction became important. The observed $C_{aromatic}$−H shifts are probably due to changes in the H-bond strength and the relative contribution of the overlapping Fermi resonance bands. Moreover, the force balance between Coulombic and van der Waals interactions, relative to the number of $-CH_2-$ groups, is also expressed by the decrease of the T_m and the increase of the T_g. Studies using PILs and alkali NTf_2^- melts have elucidated the effect of different types of interactions on the conformational isomerism of the anion (expressed by the ΔH_{eq}). In environments in which Coulombic interactions are predominant, the most probable NTf_2^- conformer is the *trans* conformer, while when other types of interactions (HB, vdW, etc.) become important the *cis* conformer is favored. Furthermore, the NTf_2^- conformational equilibrium follows quite well the relative strength of these interactions, as evidenced by the structural changes observed in the PILs studied. Finally, in a recent theoretical work, it was shown that the anion could be the "reporter" of the ILs' structure.[49] This work supports this view[49] using a different approach, compared to neutron/X-ray scattering used in the past. We also extend it by showing that in each case the right property/descriptor has to be identified and measured using an appropriate technique in order to conclude about the local ILs' structure.

ASSOCIATED CONTENT

Supporting Information

Synthesis procedure and structure of aprotic ionic liquids HC_nImNTf_2 (n = 0−12) and alkali molten salts $ANTf_2$ (K and Cs), vibrational spectroscopy measurements, and calculation details. This material is available free of charge via the Internet at http://pubs.acs.org.

AUTHOR INFORMATION

Corresponding Authors

*E-mail: indy@iceht.forth.gr.
*E-mail: vlad@udel.edu.

Notes

The authors declare no competing financial interest.

ACKNOWLEDGMENTS

V.N. acknowledges support from the Catalysis Center for Energy Innovation, an Energy Frontier Research Center funded by the U.S. Department of Energy, Office of Science, Office of Basic Energy Sciences, under award number DE-SC0001004.

REFERENCES

(1) Wasserscheid, P.; Keim, W. Ionic Liquids—New "Solutions" for Transition Metal Catalysis. *Angew. Chem., Int. Ed.* **2000**, *39*, 3772−3789.
(2) MacFarlane, D. R.; Forsyth, M.; Howlett, P. C.; Pringle, J. M.; Sun, J.; Annat, G.; Neil, W.; Izgorodina, E. I. Ionic Liquids in Electrochemical Devices and Processes: Managing Interfacial Electrochemistry. *Acc. Chem. Res.* **2007**, *40*, 1165−1173.
(3) Galiński, M.; Lewandowski, A.; Stępniak, I. Ionic Liquids as Electrolytes. *Electrochim. Acta* **2006**, *51*, 5567−5580.
(4) Marszalek, M.; Fei, Z.; Zhu, D.-R.; Scopelliti, R.; Dyson, P. J.; Zakeeruddin, S. M.; Grätzel, M. Application of Ionic Liquids Containing Tricyanomethanide $[C(C_n)_3]^-$ or Tetracyanoborate $[B(C_n)_4]^-$ Anions in Dye-Sensitized Solar Cells. *Inorg. Chem.* **2011**, *50*, 11561−11567.
(5) Kerton, F. M. *Alternarive Solvents for Green Chemistry*; Royal Society of Chemistry: Cambridge, U.K., 2009.
(6) Ab Rani, M. A.; Brant, A.; Crowhurst, L.; Dolan, A.; Lui, M.; Hassan, N. H.; Hallett, J. P.; Hunt, P. A.; Niedermeyer, H.; Perez-Arlandis, J. M. Understanding the Polarity of Ionic Liquids. *Phys. Chem. Chem. Phys.* **2011**, *13*, 16831−16840.
(7) Niedermeyer, H.; Ashworth, C.; Brandt, A.; Welton, T.; Hunt, P. A. A Step Towards the a Priori Design of Ionic Liquids. *Phys. Chem. Chem. Phys.* **2013**, *15*, 11566−11578.
(8) Lehmann, S. B. C.; Roatsch, M.; Schoppke, M.; Kirchner, B. On the Physical Origin of the Cation-Anion Intermediate Bond in Ionic Liquids Part I. Placing a (Weak) Hydrogen Bond between Two Charges. *Phys. Chem. Chem. Phys.* **2010**, *12*, 7473−7486.
(9) Tokuda, H.; Ishii, K.; Susan, M. A. B. H.; Tsuzuki, S.; Hayamizu, K.; Watanabe, M. Physicochemical Properties and Structures of Room-Temperature Ionic Liquids. 3. Variation of Cationic Structures. *J. Phys. Chem. B* **2006**, *110*, 2833−2839.
(10) Fumino, K.; Wulf, A.; Ludwig, R. The Cation−Anion Interaction in Ionic Liquids Probed by Far-Infrared Spectroscopy. *Angew. Chem., Int. Ed.* **2008**, *47*, 3830−3834.
(11) Papatheodorou, G. N.; Yannopoulos, S. N. Light Scattering from Molten Salts: Structure and Dynamics. In *Molten Salts: From Fundamentals to Applications*; Gaune-Escard, M., Ed.; Nato Science Series; Kluwer Academic Press: Norwell, MA, 2002; Vol. *52*, pp 46−106.
(12) Peppel, T.; Roth, C.; Fumino, K.; Paschek, D.; Köckerling, M.; Ludwig, R. The Influence of Hydrogen-Bond Defects on the Properties of Ionic Liquids. *Angew. Chem., Int. Ed.* **2011**, *50*, 6661−6665.

(13) Russina, O.; Triolo, A.; Gontrani, L.; Caminiti, R. Mesoscopic Structural Heterogeneities in Room-Temperature Ionic Liquids. *J. Phys. Chem. Lett.* **2011**, *3*, 27−33.
(14) Noack, K.; Schulz, P. S.; Paape, N.; Kiefer, J.; Wasserscheid, P.; Leipertz, A. The Role of the C2 Position in Interionic Interactions of Imidazolium Based Ionic Liquids: A Vibrational and NMR Spectroscopic Study. *Phys. Chem. Chem. Phys.* **2010**, *12*, 14153−14161.
(15) Hunt, P. A. Why Does a Reduction in Hydrogen Bonding Lead to an Increase in Viscosity for the 1-Butyl-2,3-Dimethyl-Imidazolium-Based Ionic Liquids? *J. Phys. Chem. B* **2007**, *111*, 4844−4853.
(16) Canongia Lopes, J. N. A.; Pádua, A. A. H. Nanostructural Organization in Ionic Liquids. *J. Phys. Chem. B* **2006**, *110*, 3330−3335.
(17) Anderson, J. L.; Ding, J.; Welton, T.; Armstrong, D. W. Characterizing Ionic Liquids on the Basis of Multiple Solvation Interactions. *J. Am. Chem. Soc.* **2002**, *124*, 14247−14254.
(18) Rocha, M. A. A.; Lima, C. F. R. A. C.; Gomes, L. g. R.; Schröder, B.; Coutinho, J. o. A. P.; Marrucho, I. M.; Esperança, J. M. S. S.; Rebelo, L. s. P. N.; Shimizu, K.; Lopes, J. N. C. High-Accuracy Vapor Pressure Data of the Extended $[C_nC_1Im][NTf_2]$ Ionic Liquid Series: Trend Changes and Structural Shifts. *J. Phys. Chem. B* **2011**, *115*, 10919−10926.
(19) Verevkin, S. P.; Zaitsau, D. H.; Emel'yanenko, V. N.; Yermalayeu, A. V.; Schick, C.; Liu, H.; Maginn, E. J.; Bulut, S.; Krossing, I.; Kalb, R. Making Sense of Enthalpy of Vaporization Trends for Ionic Liquids: New Experimental and Simulation Data Show a Simple Linear Relationship and Help Reconcile Previous Data. *J. Phys. Chem. B* **2013**, *117*, 6473−6486.
(20) Fujii, K.; Fujimori, T.; Takamuku, T.; Kanzaki, R.; Umebayashi, Y.; Ishiguro, S.-i. Conformational Equilibrium of Bis-(Trifluoromethanesulfonyl) Imide Anion of a Room-Temperature Ionic Liquid: Raman Spectroscopic Study and Dft Calculations. *J. Phys. Chem. B* **2006**, *110*, 8179−8183.
(21) Herstedt, M.; Smirnov, M.; Johansson, P.; Chami, M.; Grondin, J.; Servant, L.; Lassègues, J. C. Spectroscopic Characterization of the Conformational States of the Bis(Trifluoromethanesulfonyl)Imide Anion ($TFSI^-$). *J. Raman Spectrosc.* **2005**, *36*, 762−770.
(22) Berg, R. W.; Deetlefs, M.; Seddon, K. R.; Shim, I.; Thompson, J. M. Raman and Ab Initio Studies of Simple and Binary 1-Alkyl-3-Methylimidazolium Ionic Liquids. *J. Phys. Chem. B* **2005**, *109*, 19018−19025.
(23) Moschovi, A. M.; Ntais, S.; Dracopoulos, V.; Nikolakis, V. Vibrational Spectroscopic Study of the Protic Ionic Liquid 1-H-3-Methylimidazolium Bis(Trifluoromethanesulfonyl)Imide. *Vib. Spectrosc.* **2012**, *63*, 350−359.
(24) Zhang, S.; Sun, N.; He, X.; Lu, X.; Zhang, X. Physical Properties of Ionic Liquids: Database and Evaluation. *J. Phys. Chem. Ref. Data* **2006**, *35*, 1475−1517.
(25) Bennett, C.; Kaya, E.; Sikes, A. M.; Jarrett, W. L.; Mathias, L. J. Synthesis and Characterization of Nylon 18 18 and Nylon 18 Adamantane. *J. Polym. Sci., Part A: Polym. Chem.* **2009**, *47*, 4409−4419.
(26) Paulechka, Y. U.; Blokhin, A. V.; Kabo, G. J.; Strechan, A. A. Thermodynamic Properties and Polymorphism of 1-Alkyl-3-Methylimidazolium Bis(Triflamides). *J. Chem. Thermodyn.* **2007**, *39*, 866−877.
(27) Coleman, M. M.; Painter, P. C. Hydrogen Bonded Polymer Blends. *Prog. Polym. Sci.* **1995**, *20*, 1−59.
(28) Russina, O.; Triolo, A.; Gontrani, L.; Caminiti, R.; Xiao, D.; Hines, L. G., Jr.; Bartsch, R. A.; Quitevis, E. L.; Plechkova, N.; Seddon, K. R. Morphology and Intermolecular Dynamics of 1-Alkyl-3-Methylimidazolium Bis{(Trifluoromethane)Sulfonyl}Amide Ionic Liquids: Structural and Dynamic Evidence of Nanoscale Segregation. *J. Phys.: Condens. Matter* **2009**, *21*, 424121.
(29) Triolo, A.; Russina, O.; Fazio, B.; Appetecchi, G. B.; Carewska, M.; Passerini, S. Nanoscale Organization in Piperidinium-Based Room Temperature Ionic Liquids. *J. Chem. Phys.* **2009**, *130*, 164521.
(30) Rocha, M. A. A.; Coutinho, J. A. P.; Santos, L. M. N. B. F. Evidence of Nanostructuration from the Heat Capacities of the 1,3-Dialkylimidazolium Bis(Trifluoromethylsulfonyl)Imide Ionic Liquid Series. *J. Chem. Phys.* **2013**, *139*, 104502.
(31) Ricard, L.; Abbate, S.; Zerbi, G. Conformationally Dependent Fermi Resonances and Long-Range Interactions Between.Sigma. Bonds in Polymethylene Systems Derived from Their Raman Spectra. *J. Phys. Chem.* **1985**, *89*, 4793−4799.
(32) Abbate, S.; Wunder, S. L.; Zerbi, G. Conformational Dependence of Fermi Resonances in N-Alkanes. Raman Spectrum of 1,1,1,4,4,4-Hexadeuteriobutane. *J. Phys. Chem.* **1984**, *88*, 593−600.
(33) Zerbi, G.; Magni, R.; Gussoni, M. Spectroscopic Markers of the Conformational Mobility of Chain Ends in Molecules Containing N-Alkane Residues. *J. Mol. Struct.* **1981**, *73*, 235−237.
(34) Zerbi, G.; Magni, R.; Gussoni, M.; Moritz, K. H.; Bigotto, A.; Dirlikov, S. Molecular Mechanics for Phase Transition and Melting of N-Alkanes: A Spectroscopic Study of Molecular Mobility of Solid N-Nonadecane. *J. Chem. Phys.* **1981**, *75*, 3175−3194.
(35) Lassègues, J.-C.; Grondin, J.; Cavagnat, D.; Johansson, P. New Interpretation of the CH Stretching Vibrations in Imidazolium-Based Ionic Liquids. *J. Phys. Chem. A* **2009**, *113*, 6419−6421.
(36) Grondin, J.; Lassègues, J.-C.; Cavagnat, D.; Buffeteau, T.; Johansson, P.; Holomb, R. Revisited Vibrational Assignments of Imidazolium-Based Ionic Liquids. *J. Raman Spectrosc.* **2011**, *42*, 733−743.
(37) Wulf, A.; Fumino, K.; Ludwig, R. Comment on "New Interpretation of the Ch Stretching Vibrations in Imidazolium-Based Ionic Liquids". *J. Phys. Chem. A* **2009**, *114*, 685−686.
(38) Lassègues, J.-C.; Grondin, J.; Cavagnat, D.; Johansson, P. Reply to the "Comment on 'New Interpretation of the CH Stretching Vibrations in Imidazolium-Based Ionic Liquids'". *J. Phys. Chem. A* **2009**, *114*, 687−688.
(39) Roth, C.; Chatzipapadopoulos, S.; Kerlé, D.; Friedriszik, F.; Lütgens, M.; Lochbrunner, S.; Kühn, O.; Ludwig, R. Hydrogen Bonding in Ionic Liquids Probed by Linear and Nonlinear Vibrational Spectroscopy. *New J. Phys.* **2012**, *14*, 105026.
(40) Obi, E. I.; Leavitt, C. M.; Raston, P. L.; Moradi, C. P.; Flynn, S. D.; Vaghjiani, G. L.; Boatz, J. A.; Chambreau, S. D.; Douberly, G. E. Helium Nanodroplet Isolation and Infrared Spectroscopy of the Isolated Ion-Pair 1-Ethyl-3-Methylimidazolium Bis-(Trifluoromethylsulfonyl)Imide. *J. Phys. Chem. A* **2013**, *117*, 9047−9056.
(41) Cooper, R.; Zolot, A. M.; Boatz, J. A.; Sporleder, D. P.; Stearns, J. A. Ir and Uv Spectroscopy of Vapor-Phase Jet-Cooled Ionic Liquid $[Emim]+[Tf_2n]^-$: Ion Pair Structure and Photodissociation Dynamics. *J. Phys. Chem. A* **2013**, *117*, 12419−12428.
(42) Katsyuba, S. A.; Vener, M. V.; Zvereva, E. E.; Fei, Z.; Scopelliti, R.; Laurenczy, G.; Yan, N.; Paunescu, E.; Dyson, P. J. How Strong Is Hydrogen Bonding in Ionic Liquids? Combined X-Ray Crystallographic, Infrared/Raman Spectroscopic, and Density Functional Theory Study. *J. Phys. Chem. B* **2013**, *117*, 9094−9105.
(43) Namboodiri, M.; Kazemi, M. M.; Zeb Khan, T.; Materny, A.; Kiefer, J. Ultrafast Vibrational Dynamics and Energy Transfer in Imidazolium Ionic Liquids. *J. Am. Chem. Soc.* **2014**, *136*, 6136−6141.
(44) Kossmann, S.; Thar, J.; Kirchner, B.; Hunt, P. A.; Welton, T. Cooperativity in Ionic Liquids. *J. Chem. Phys.* **2006**, *124*, 174506−174512.
(45) Joseph, J.; Jemmis, E. D. Red-, Blue-, or No-Shift in Hydrogen Bonds: A Unified Explanation. *J. Am. Chem. Soc.* **2007**, *129*, 4620−4632.
(46) Alabugin, I. V.; Manoharan, M.; Peabody, S.; Weinhold, F. Electronic Basis of Improper Hydrogen Bonding: A Subtle Balance of Hyperconjugation and Rehybridization. *J. Am. Chem. Soc.* **2003**, *125*, 5973−5987.
(47) Mignon, P.; Loverix, S.; Geerlings, P. Interplay between $\pi-\pi$ Interactions and the H-Bonding Ability of Aromatic Nitrogen Bases. *Chem. Phys. Lett.* **2005**, *401*, 40−46.
(48) Hardacre, C.; Holbrey, J. D.; Mullan, C. L.; Youngs, T. G. A.; Bowron, D. T. Small Angle Neutron Scattering from 1-Alkyl-3-Methylimidazolium Hexafluorophosphate Ionic Liquids ($[C_nmim][Pf_6]$, N = 4, 6, and 8). *J. Chem. Phys.* **2010**, *133*, 074510−074517.

(49) Hettige, J. J.; Kashyap, H. K.; Annapureddy, H. V. R.; Margulis, C. J. Anions, the Reporters of Structure in Ionic Liquids. *J. Phys. Chem. Lett.* **2012**, *4*, 105−110.